Indian Journal of Pure & Applied Physics
Vol. 62, September 2024, pp. 733-742
DOI: 10.56042/ijpap.v62i9.11726

Enhanced Acetone Detection Using Nano NaA Zeolite: A Study on Optical and Dielectric Properties

Malikarjun Wakade[a,b] & Megha Mahabole[b*]

[a]Shivneri Mahavidyalaya, Shirur Anantpal, Dist Latur 413 544 MS, India

[b]School of Physical Sciences, Swami Ramanand Teerth Marathwada University, Nanded 431 606, MS, India

Received 12 June 2024; accepted 1 August 2024

The increasing presence of toxic gases, particularly acetone, poses significant threats to both the environment and human health. Effective detection of acetone is crucial, necessitating the development of reliable and sensitive sensors. This study explores the use of Nano NaA zeolite as a promising material for acetone sensing, leveraging its excellent adsorption and desorption properties. Comprehensive material characterization is performed using X-ray Diffraction (XRD), Fourier Transform Infrared Spectroscopy (FTIR), Thermogravimetric Analysis-Differential Thermal Analysis (TG-DTA), Scanning Electron Microscopy (SEM), Energy Dispersive X-ray Analysis (EDAX) and Atomic Force Microscopy (AFM). The sensing characteristics of Nano NaA zeolite are rigorously evaluated. The sensor exhibits optimal performance at an operating temperature of 75 °C, with a response time of 88 seconds and a recovery time of 75 seconds. The sensor demonstrates excellent sensitivity at a saturation concentration of 85 ppm. Repeatability tests conducted over three trials confirmes the sensor's consistent performance, while durability assessments conducted over a 30-day period (with measurements after every 5 days) highlights its long-term stability. Additionally, the study investigates the effect of acetone exposure on optical and dielectric properties of the sensor. This research underscores the potential of Nano NaA zeolite as an effective acetone sensor, offering valuable insights into its optical and dielectric properties. The findings support the development of robust and durable acetone sensors for environmental monitoring and human safety.

Keyword: Acetone Sensor; Nano NaA zeolite; Optical properties; Dielectric properties; Material characterization

1 Introduction

The term "air pollution" describes the discharge of contaminants into the atmosphere that are harmful to both the environment and human health[1,2]. The significance of sensitive gas monitoring in the identification of pollutants and air quality testing is growing. This is particularly true when it comes to the detection of oxidizing gases, which are the primary by products of burning fossil fuels and reducing gases namely acetone, nitrogen dioxide (NO_2), carbon monoxide, carbon dioxide, hydrogen sulphide and sulphur dioxide[3-5]. Acetone (C_3H_6O) is one of the colourless, flammable and explosive and transparent volatile organic compounds that is frequently being used in industries, laboratories and pharmaceutical plants. It is a poisonous, hazardous, and damaging gas. It is extremely unstable and can seriously effects on human biology and health. Acetone inhalation can be detrimental to the neurological system and result in headaches, allergies, exhaustion, and even narcosis[9–12]. Long term exposure to high acetone concentrations can damage the eyes. Therefore, it is crucial to keep an eye on the amount of acetone present in the surroundings and also at work place for safety reasons. Furthermore, as living standards have increased recently, sophisticated dietary and lifestyle modifications have resulted in an increase in a number of ailments[13]. One of the illnesses that is spreading quickly is diabetes. Acetone is employed as a potential biomarker for non-invasive diabetes diagnosis and detection[14]. A vast number of clinical data analyses demonstrate that the acetone concentration in the exhaled breath of diabetes patients is typically greater than 1.8 ppm, whereas the concentration of acetone gas in the exhaled breath of healthy people is less than 0.9 ppm[23-25]. This technology for sensing exhaled air can be used to monitor patients in real time and is gaining popularity in medical applications. Therefore, it is essential to develop acetone sensors for health monitoring and self-diagnosis applications. However, the exhaled air of the human body is a very complex environment. Detecting trace concentrations of target analytes in

*Corresponding author:
(E-mail: pmahabole14@gmail.com)

high humidity environments is a significant difficulty. As a result, there is an urgent need to design a gas sensor that performs well in high humidity environments[26,27]. Thus, it is important to explore materials with special structure for their use in sensor area. The easiest and reliable way is to use porous materials.

NaA zeolite is an important family member of highly porous, crystalline aluminosilicate materials. Zeolite consists of tetrahedral TO_4 building blocks (T = Si, Al, etc.). Tetrahedral TO_4 units are linked together by the distribution of oxygen atoms to create three-dimensional crystalline spongy skeletons. The T-O-T linkages provide a variety of rings, which are suitable for zeolites' cages and channels with varying window widths. Within the skeleton arrangement, the aluminum atom in the center of an AlO_4 tetrahedra connects to silicon atom of an adjacent SiO_4 tetrahedra by sharing an O atom, generating a negative framework charge that is balanced by the transferable cations residing in cages, such as an alkaline or alkaline-earth cations, resulting in the property of ion exchange[15]. Ion exchange with various cations can modify zeolites' pore size, ion conductivity, adsorption, and catalytic selectivity. The goal of utilizing zeolites in sensors is typically to increase sensitivity and selectivity by preferential adsorption; also, films ensure a short reaction time for the sensor. The pores and cages with certain window widths inside a zeolite's architecture allow some molecules to pass through while others are ejected. Zeolites with a porous structure can filter out molecules with molecular diameters larger than the zeolites' pores. A high concentration of cations in zeolite generates a strong electrostatic field in the pores, which easily adsorbs polar molecules, resulting in a significantly higher concentration of absorbed polar molecules in the pores than on the pores' exterior surface. Second, these cations play a significant function in the acid catalysis of zeolites; the acidity of the zeolites can be regulated by varying the species and number of cations present. Moreover, porous structure offers high surface area beneficial for adsorption of gas molecules. Based on these properties, numerous varieties of zeolites have been employed to increase the performance of gas sensors. Covering a kind of A-zeolite over Pd-doped SnO_2-sensitive materials substantially inhibited the reactions to acetone, carbon monoxide, H_2, CH_4, and C_3H_8, while retaining a strong sensitivity to ethanol[16]. Acetone gas has been successfully detected using a QCM sensor with Ag-ZSM-5 zeolite as the sensitive material, with a minimum detection concentration of less than 1 ppm[17]. A WO_3 sensor modified with zeolite has shown significant increase in NO_2 detection characteristics[18]. The enhancement in responses and selectivity to various VOCs has been observed for a SnO_2 sensor modified with zeolites such as LTA, FAU, and MFI[19]. Moos et al have developed H-ZSM-5 zeolite sensor for managing selective catalytic reduction (SCR) systems and detecting ammonia leakage[20].

In addition, Il-Doo Kim et al have reported a MOFs-derived n-type SnO_2 (n-SnO_2) sensing layer functionalized by cocatalysts (PdO NPs and Co_3O_4 islands) to detect acetone vapour with a gas response value of 22.8 (R_{air}/R_{gas}) towards 5 ppm acetone at 90% RH and 450 °C[28]. Won-Tae Koo and group have developed MOF-derived synergistic catalysts that are functionalized with hollow SnO_2 nanotubes (NTs) wherein a high acetone response (R_{air}/R_{gas} = 5.06 at 400 °C @ 1 ppm) and a quick response (20 s) and recovery (64 s) time is observed in a very humid environment (95% RH)[29]. Furthermore, Xudong Cui et al have developed porous ZnO/Co_3O_4 composites by direct pyrolysis of MOF precursors. This produced ZnO/Co_3O_4 sample has shown higher sensitivity (15.17 ppm−1) at 275 °C[30]. According to literature survey, acetone sensors have shown promising performances for usage in practical applications, but they still suffer from issues such as high operating temperatures and extended response/recovery times. As a result, development of appropriate low-temperature gas detecting devices are essential in the sensor industry.

In this work, NaA zeolite thick film sensors have been developed due to its porous nature, high surface area and excellent adsorption properties. Therefore, attempt has been made to employ the NaA zeolite as a sensing material to construct low temperature acetone sensor with excellent sensitivity, short response/ recovery time, good reversibility and durability. Also, the optical and dielectric properties of sensor material are carried out just to ensure adsorption of gas.

2 Experimental Method

2.1 Material preparation and characterization techniques

NaA zeolite and acetone, used in this experiment, are procured from Sigma Aldrich and S.D. Fine Chemical Limited (SDFCL) respectively and are used

without further purification. A thorough analysis of NaA zeolite is required to determine its appropriateness for acetone sensing applications. Therefore, NaA zeolite's structural, functional, thermal, morphological, optical, and dielectric characteristics are evaluated using a variety of analytical methods. The crystalline structure is determined using Rigaku make X-ray diffractometer (XRD) in the 2θ range of 10° to 60°. While Fourier transform infrared spectroscopy (FTIR) is employed to reveal information about the material's chemical bonds and functional groups. Thermogravimetric Analysis/Differential Thermal Analysis (TG-DTA) is carried out with the help of Shimadzu make thermal analyzer to evaluate thermal stability, while scanning electron microscopy (SEM) is used to observe the surface morphology, shape and particle size distribution.

2.2 Thick film preparation

The screen-printing method is used to create the thick film sensors, as described in earlier work[31]. This method involves mixing of NaA zeolite with binders such glass frit, ethyl cellulose, and viscous butyl carbitol acetate (BCA) to create a thixotropic paste. This is followed by careful deposition of paste on precleaned glass substrate using screen. A squeegee is used to push the paste through a porous mesh screen. The finished film has dimensions of (1x2) cm². After deposition, the coated films are dried for 20 minutes under an infrared light to get rid of the temporary binders. The dried films are then allowed to anneal in air with the help of programmable furnace. In order to improve the structural integrity of the film and guarantee that the NaA zeolite particles adhered well, an annealing phase is carried out for two hours at 550 °C. Finally, deposited thick film sensors are used for additional testing.

2.3 Gas sensing performance

The performance of each developed sensor for detecting acetone is evaluated using an indoor stationary gas sensor unit. The thick film sensor is mounted on a heating element inside the chamber, with a thermocouple in direct contact with the substrate to monitor its temperature. Electrical measurements are facilitated by connecting copper electrodes to the substrate material using a two-probe technique. Initially, the substrate is preheated in the sensing chamber to mitigate humidity effects. During the experiment, the sensor's temperature is varied from room temperature to 200 °C, and its resistance is recorded as a function of temperature in an air atmosphere. After this, a fixed concentration of acetone (2 ppm) is introduced into the dome through a small aperture regulator, and the resistance is measured at specific temperature intervals. The relative change in resistance is calculated using the following formula[31-33].

$$Gas\ response\ S(\%) = \frac{R_g - R_a}{R_a} \times 100 \quad \ldots (1)$$

Where Rg and Ra are the resistances of sensor in gas and air atmoshre atmospheres.

In this study, the optimal operating temperature for NaA zeolite thick film sensor is identified by plotting the response to acetone vapors against temperature and confirmed through repeatability test. Additionally, response and recovery times are determined by alternately exposing the film to a fixed concentration of acetone vapors and fresh air. Also, he maximum uptake capacity of the sensor film, is also determined to assess the performance of sensor film. The uptake capacity is measured for various acetone concentrations, ranging from 2 ppm to saturation value, while maintaining the sensor at its optimal operating temperature. The stability of sensor is evaluated by exposing it to 2 ppm acetone at regular intervals of 5 days for 30 days and by plotting sensitivity vs duration graph.

2.4 Ultraviolet-Visible Spectra

A Shimadzu make spectrophotometer is used for examining optical characteristics using UV-Visible spectroscopy. The wavelength range of 300 nm to 800 nm is selected to record spectra, which provides information about the materials' optical property. The Tauc equation is used for determining the energy band gap:

$$\alpha h\nu = A(h\nu - E_g)_2^1 \quad \ldots (2)$$

2.5 Dielectric study

In the current study, dielectric measurements are conducted on NaA zeolite at room temperature. Initially, NaA powder sample is compacted into pellet form at a pressure of 5 tons using hydraulic press. To carry out measurements, silver paste is applied to both surfaces of the pellet sample to have proper electrical contacts. Various parameters namely Cp, Df, Rs, and

Xs are recorded as a function of frequency in the range of 10Hz to 2 MHz with the help of Quad Tech make 7600 precision LCR meter. The dielectric constant is calculated using the following formula (Eq. 3)

$$\varepsilon' = \frac{C_p \times t}{\varepsilon_0 \times A} \quad \ldots (3)$$

Where A is the area of the cross section of the sample pellet, C_p is the capacitance of the sample, t is its thickness, $\varepsilon_0$is the permittivity of free space.

AC conductivity is calculated using the following formula (Eq. 4);

$$\sigma = \frac{(Z')^2}{(Z')^2+(Z'')^2} \times \frac{t}{A} \quad \ldots (4)$$

In this context, Z′ represents the real part of the impedance, Z″ denotes the imaginary part of the impedance, t is the thickness of the plate, and A is the area of the pellet.

The variations in dielectric constant and AC conductivity are plotted against frequency. Additionally, Cole-Cole plots are also presented and analyzed for NaA zeolite.

3 Results and Discussion

3.2 Analysis by X-ray Diffraction

Figure 1(a) displays the X-ray diffraction (XRD) pattern of NaA zeolite. It is recorded over the 2θ range of 10° to 60°. Presence of sharp peaks ensures highly crystalline structure of NaA. The XRD analysis carried out with the help of standard

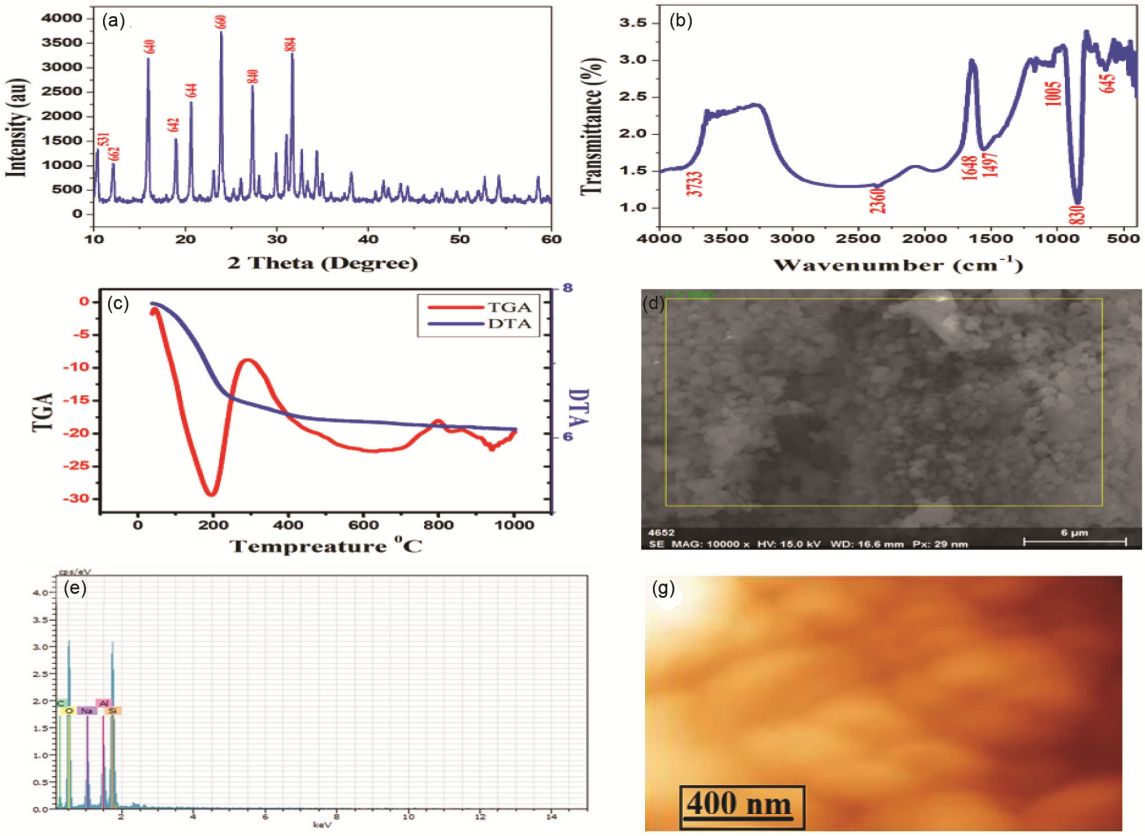

(f)

El	AN	Series	unn. C [wt.%]	norm. C [wt.%]	Atom. C [at.%]	Error (1 Sigma) [wt.%]
O	8	K-series	49.24	51.80	58.26	7.58
Si	14	K-series	19.99	21.03	13.48	0.92
C	6	K-series	10.51	11.05	16.56	3.18
Na	11	K-series	7.80	8.20	6.42	0.59
Al	13	K-series	7.52	7.91	5.28	0.43
		Total:	95.06	100.00	100.00	

Fig. 1 — Characteristics of NaA Zeolite; (a) X-ray profile, (b) FTIR Spectra, (c) TG-DTA plot (d) Scanning electron microscopy, (e) Elemental analysis, (f) Elemental composition and (g) Atomic force microscopy

reference data (74-1183-JCPDS-ICDD, 2001) confirms the occurrence of typical diffraction peaks for NaA zeolite at 2θ values of 10.19°, 12.48°, 16.13°, 18.97°, 20.71°, 24.06°, 27.31° and 31.85°, These peaks correspond to crystallographic planes such as (531), (662), (640), (642), (644), (660), (840), and (880) respectively indicating the tetragonal phase of NaA zeolite. The average particle size of NaA zeolite, calculated using Debye-Scherrer's formula, is observed to be approximately 66 nm[31].

3.2 Analysis of Fourier transform infrared spectrum

Figure 1(b) illustrates the Fourier transform infrared (FT-IR) spectrum of NaA zeolite, recorded within the wavenumber range of 400 to 4000 cm^{-1}. The spectrum features a characteristic band at 664 cm^{-1} which can be attributed to the symmetric stretching vibrations of the T (Si, Al)-O bonds within the zeolite framework. Another notable absorption band, appearing at 1005 cm^{-1}, corresponds to the internal vibrations of the T-O bonds. Additionally, peaks at 1497 cm^{-1} and 1648 cm^{-1} can be assigned to the internal tetrahedral symmetrical stretching and the external linkage asymmetrical stretching, respectively. The peak observed at 2360 cm^{-1} is associated with the bending vibrations of the internal (TO□) tetrahedral structures. Furthermore, a distinct band at 3733 cm^{-1} is indicative of the absorbed, isolated, mono-coordinated OH groups[31].

3.3 Thermogravimetric-Differential Thermal Analysis

Figure 1(c) presents the TG-DTA curve of NaA zeolite. The initial weight loss occurring between 100 to 200 °C is due to the removal of hydroxyl groups observed on surface. The second weight loss happening between 200 to 300 °C may be due to gradual initiation of removal of water molecules residing in cages and voids in a NaA zeollite structure *i.e.* initiation of dehydration of hydrated sodium A zeolite[31].

These results are well supported by DTA. The curve shows the existence of an endothermic peak near about 200 °C corresponding to release of adsorbed water molecules. A prominent exothermic peak at 300 °C indicates the evaporation of zeolitic water molecules present in structure, marking the beginning of the material's decomposition. Beyond this temperature, the DTA curve suggests the completion of decomposition in the material[31].

3.4 Scanning Electron Microscopy

Figure 1(d) indicates the SEM image of NaA zeolite. The observed morphology shows that particles appear mostly cubic in shape. which is the characteristic morphology of NaA zeolite crystals. However, the some irregularly shaped and different sizes particles are present as well. The smallest grain observed in the micrograph are of 0.20 nm and larger grains are of 2-micron size. The average grain size of sample material is 66.24 nm which matches with x-ray diffraction results[31].

3.5 Energy Dispersive X-ray Analysis

Figure 1(e) presents EDS spectrum. It is utilized to determine the elemental composition of NaA zeolite. The EDAX spectrum offers both qualitative and quantitative insights into the elements present within the sample. Typically, the composition of NaA zeolite includes silicon (Si), aluminum (Al), sodium (Na), and oxygen (O). These elements confirm the chemical makeup of the zeolite, consistent with its aluminosilicate framework. The peaks corresponding to these elements are observed to be present in spectrum.

The Table (Fig. 1(f)) presents the elemental composition of NaA zeolite as determined by Energy Dispersive X-ray Analysis (EDAX). This technique is used for identification of elemental makeup of materials. The "K-series" notation indicates the specific X-ray emission lines used to detect each element. The main elements identified in the sample are silicon (Si), aluminum (Al), sodium (Na), and carbon (C), which align with the expected composition of NaA zeolite ($Na_{12}Al_{12}Si_{12}O_{48}27H_2O$). This confirms that the material used is a zeolite material.

3.6 Atomic force microscopy

Figure 1(g) shows that AFM image of NaA zeolite. It is conducted in non-contact mode using silicon tips at a room temperature of around 25 °C. The AFM image reveals nanometer-scale features on the porous surfaces of NaA zeolite. Notably, pore sizes exceeding 200 nm were identified between the clusters of zeolite grains. These large pores provide extensive adsorption sites, making the material highly effective for gas adsorption. The significant porosity observed is beneficial for applications such as gas sensing and catalysis, where a large surface area and accessible adsorption sites are essential. The nanometer-sized features and substantial pore sizes helps to enhance the material's interaction with various molecules, thereby improving its performance in these applications[34].

4 Gas Sensing Performance

4.1 Operating Temperature

Operating temperature is a crucial parameter for gas sensors, as it significantly affects their efficiency. Fig. 2(a) presents the change in sensitivity with temperature which indicates the sensitivity of sensor towards acetone. It is observed that sensitivity increases with temperature and becomes maximum at specific temperature. Again, it decreases with further increase in temperature. The sensing performance of NaA zeolite thick film for acetone vapors reveals that it achieves maximum sensitivity (85%) at an operating temperature of 75 °C. This illustrates that NaA zeolite thick film sensor can effectively sense acetone at this optimal temperature.

In gas sensing process, target gas molecules interact with surface atoms via adsorption of gas molecules on adsorbent surface during exposure. Maximum sensitivity is related to large interactions with active sites which in turn depends on availability of active adsorption sites. This ensures presence of more active sites at 75 °C than at other temperatures.

4.2 Response and Recovery Time

Figure 2(b) shows response and recovery behaviour of NaA zeolite sensor after introduction of acetone. The NaA zeolite thick film demonstrates commendable performance in acetone vapor detection, particularly highlighted by its response and recovery times at an optimal operating temperature of 75 °C. The response time, which measures how quickly the sensor detects presence of acetone molecules, is recorded to be 88 seconds. Equally important is the recovery time, which is the duration needed for the sensor to return to its baseline state after acetone removal. After 75 seconds, the sensor quickly resets and prepare itself for subsequent detections without significant downtime. This efficient recovery is crucial for applications requiring continuous monitoring, ensuring the sensor maintains high sensitivity and accuracy over repeated use. The effective adsorption and desorption properties of the NaA zeolite thick film contribute to these optimal response and recovery times, enhancing its practical utility in acetone sensing applications.

4.3 Active region

The variation in sensitivity with respect to acetone gas concentration is illustrated in Fig. 2(c). The data highlights the active sensing region for acetone concentration ranging from 2 ppm to 170 ppm. This

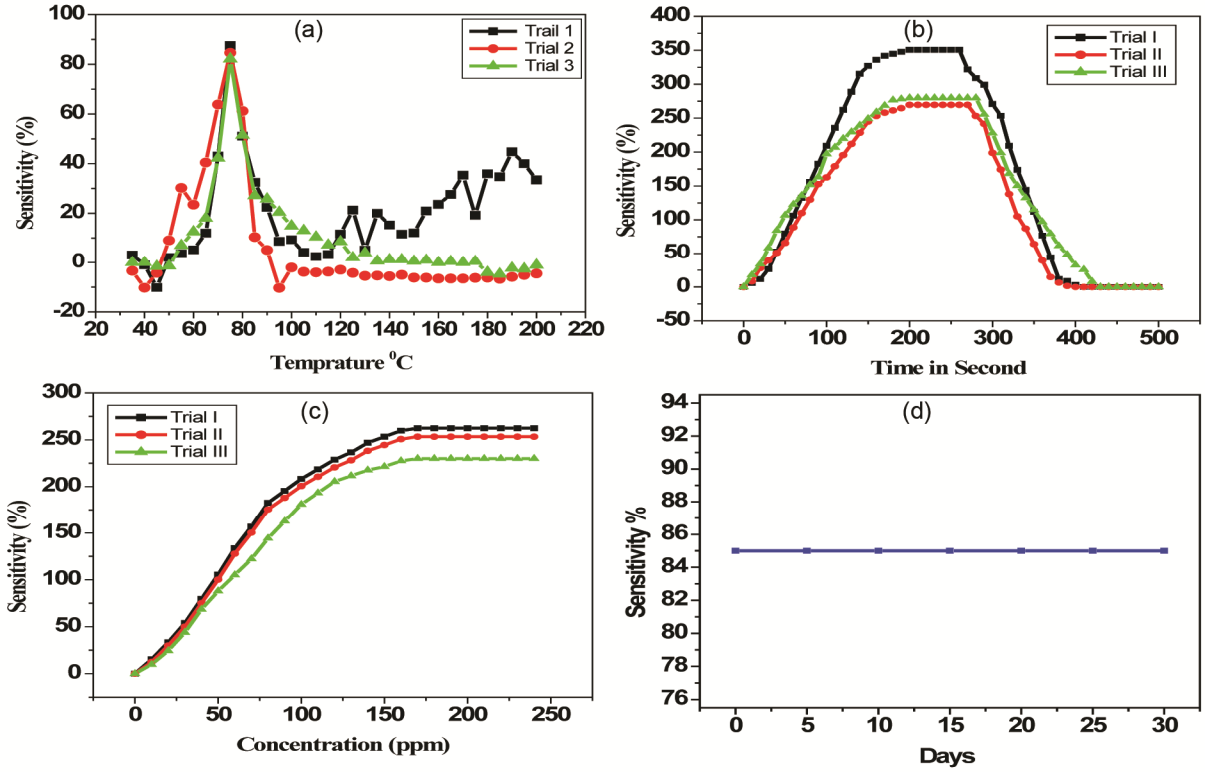

Fig. 2 — Sensing characteristics of NaA Zeolite; (a) Operating temperature, (b) Response and recovery time, (c) Active region and (d) Sensor stability

range is critical for applications requiring precise acetone detection, as it encompasses the concentrations typically encountered in various practical scenarios. At lower acetone concentrations, starting from 2 ppm, the sensor exhibits a noticeable change in sensitivity, indicating its capability to detect even minimal amounts of acetone vapor. As the concentration increases, the sensitivity factor rises correspondingly and demonstrates the sensor's robustness and reliability in tracking higher levels of acetone. The upper limit of 170 ppm represents the sensor's saturation point, beyond which further increases in acetone concentration do not significantly enhance the sensitivity factor. This saturation behavior is essential for understanding the sensor's limitations and ensuring it operates within its optimal range for accurate readings.

The sensitivity depends on presence active sites on the adsorbent surface. When the gas concentration is small, all active sites are not occupied and therefore sensitivity is observed to be very small. As the concentration increases, more and more sits get occupied which results in higher sensitivity. For further increase in concentration, sensitivity reaches to maximum and response saturates as no sites remain vacant for further adsorption to take place.

4.4 Durability

Figure 2(d) provides information about stability of NaA zeolite sensor towards acetone. It exhibits constant sensitivity throughout the 30-day of testing period after a gap of 5 days. This means the sensor maintains its ability to detect acetone at the same level for the entire duration, suggesting excellent durability. This consistent performance is ideal for reliable and long-term acetone monitoring applications.

5 UV Visible Spectroscopy

Figure 3(a) displays the variation in absorbance as a function of wavelength. The UV-Vis spectra recorded, before and after exposure to acetone gas, show considerable changes. This suggests remarkable interactions between the zeolite surface and acetone molecules. The absorption increases with exposure to test gas. This may be due to a shift in the electronic transitions within the material. Approximately 4 times increase is observed due to adsorption of gas acetone gas molecules. The appearance of new absorption peaks may be due to two main factors: first, light is absorbed by acetone molecules themselves; second, the interaction between acetone and the zeolite alters the zeolite's electronic structure.

Figure 3(b) depicts Tauc's plot indicating change in energy gap values before and after interaction of acetone molecules with sensor. The band gap for unexposed sensor is observed to be 2.0 eV while the value of energy gap reduces to 1.6 eV during acetone exposure. This reduction in band gap can be interpreted in number of ways. The presence of acetone molecules maybe responsible for increase electron excitation across the band gap, reducing the energy required for electronic transitions. Furthermore, this interaction might result in the development of new energy levels within the band gap, indicating the observed reduction in energy values. Thus, spectral changes provide information on the fundamental mechanisms guiding acetone-zeolite interaction. The changes in absorption and energy gap values emphasize the responsiveness of acetone sensor material which is important for understanding its sensing capabilities and optimizing its performance for practical applications.

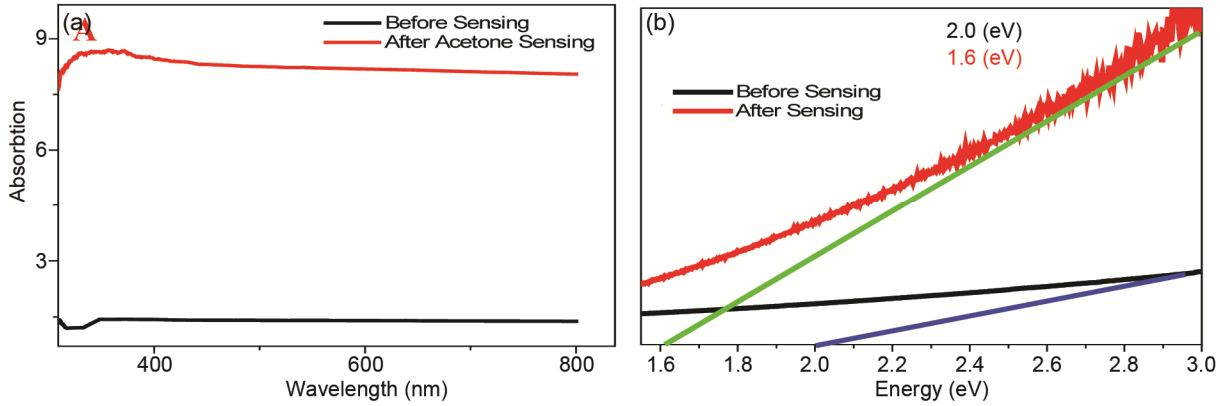

Fig. 3 — (a) UV visible spectra of before and after acetone sensing of NaA zeolite, (b) Tauq plot or Energy band gap of before and after acetone sensing of NaA zeolite

6 Dielectric Study

6.1 Dielectric constant / Permittivity

Figure 4(a) presents the change in dielectric constant for NaA zeolite with varying frequencies of an applied AC field wherein with the dielectric constant for NaA zeolite serving as the reference. It is compared with the dielectric constant after exposure to acetone. Both the curves show same trend of decrease in dielectric constant with frequency. The dielectric constant for NaA zeolite is observed to be 35 and it decreases with increasing frequency, stabilizing at higher frequencies. After introduction to acetone gas, the dielectric constant dramatically increases to 5000 following the same trend of decreasing value with frequency and frequency independent behaviour at higher frequencies. This comparison highlights the significant impact of acetone sensing on the dielectric properties of NaA zeolite.

NaA zeolite exhibits very peculiar framework structure wherein internal cavities and channels of discrete sizes and shapes are present. These channels and voids are normally occupied by water molecules, and the alkali or alkaline earth metal cations to balance the negative charge of the framework. These extra framework cations, present in the channels, are mobile. Thus, zeolite being ionic material, the total polarization is ionic in nature. When such material is placed in ac field, the heavier ions give less rapid response to applied alternating field. The observed decrease in dielectric constant is due to the fact that with the increase in frequency, the ionic displacement begins to lag the field reversals and contribute less to the dielectric constant. As a result, charges accumulate in the space charge region at the grain boundary due to the net polarization effect. At still higher frequencies the field reversals are very fast, and the ions dis placements cannot follow the field alterations. Therefore, no excess ions can accumulate in the electric field direction and ionic polarization decreases. Hence, the dielectric constant decreases with increase in frequency of applied ac field. The increase in dielectric constant after exposure to acetone gas may be due to contribution from adsorbed

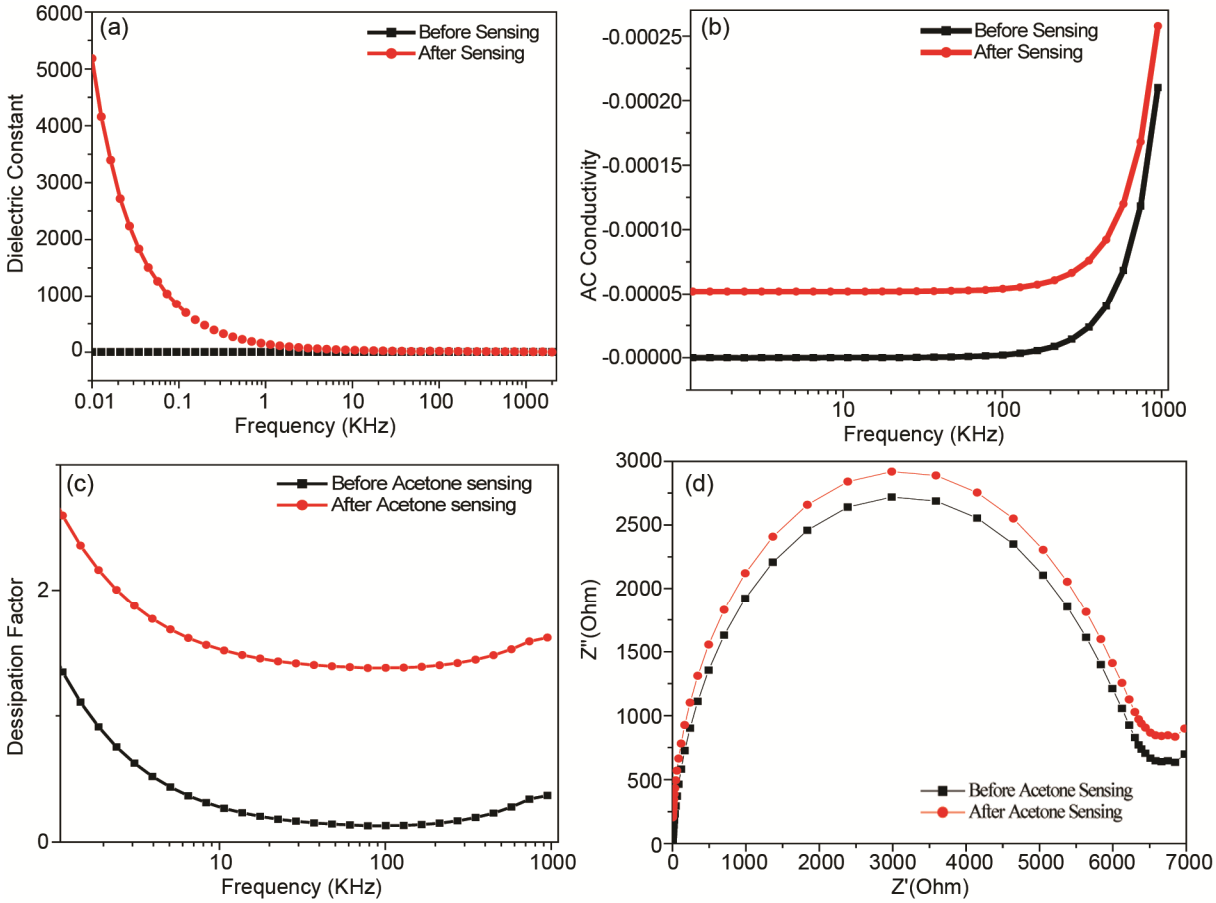

Fig. 4— (a-d) shows the dielectric performance of developed NaA zeolite sensor before and after acetone revelation.

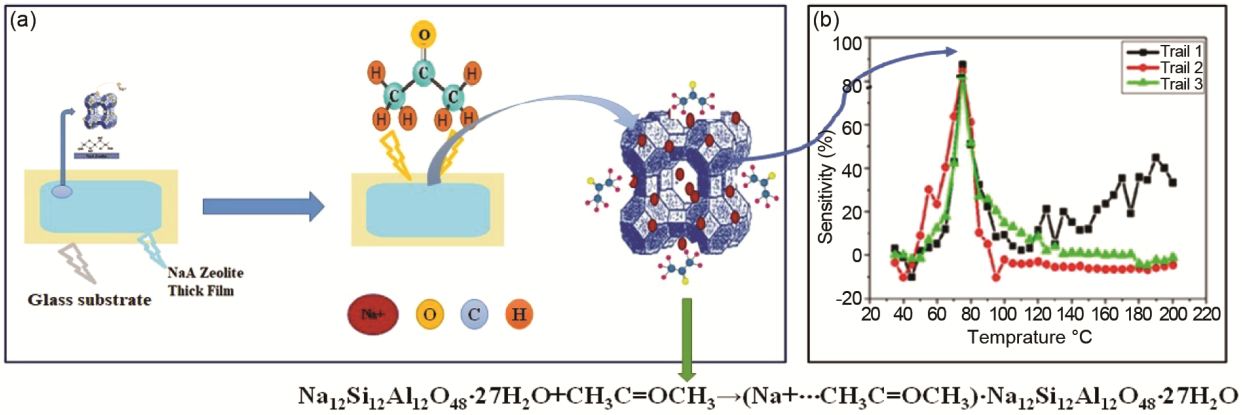

Fig. 5 — Gas sensing mechanism of acetone sensor with NaA zeolite

molecules. Bulkiness and heaviness of the material, due to adsorbed molecules, may be the reason behind decrease in dielectric constant with frequency of ac field as it becomes difficult for bulky molecule to follow field reversals.

6.2 AC conductivity

Figure 4(b) illustrates the variation of AC conductivity with frequency ranging from 10 Hz to 1 MHz for NaA zeolite before and after acetone exposure. Both the curves exhibit similar scenarios. Initially, in the low-frequency region, the AC conductivity remains relatively constant, followed by an upward shift in high frequency region. Thus, in the high-frequency region, the AC conductivity diverges from the plateau and increases linearly with frequency, following the universal power law. This increase in conductivity may be due to the hopping of charge carriers, a phenomenon commonly observed in zeolite materials. It is observed that the value of AC conductivity increases after adsorption of acetone molecules indicating presence of more charge carriers for hopping mechanism to take place from one lattice to other.

6.3 Dissipation Factor

The change in imaginary component of the dielectric constant, or dissipation factor with frequency, before and after interaction of acetone molecules with NaA zeolite, is illustrated in Fig. 4(c). In both cases, the dielectric loss exhibits dielectric dispersion with increasing frequency. The lowest dissipation factor measured for systems before acetone introduction is found to be around 1.4 whereas it climbs to approximately 2.4 following interaction of acetone molecules.

6.4 Cole- Cole Plots

Figure 4(d) depicts the Cole-Cole plots for NaA zeolite, both, before and after acetone adsorption. Cole–Cole profiles exhibit the semicircular arcs indicative of a single relaxation time, reflecting a relatively uniform dielectric response with a small tail in low frequency region in air and (air + acetone) atmospheres. These perfect semicircles indicate only one mechanism of polarization. In presence of acetone gas, the profile changes to more pronounced semicircular arc with a larger diameter. This suggests an increase in dielectric relaxation. This change indicates enhanced polarization effects and increased dielectric constant due to acetone interaction. The increased arc diameter after post-acetone sensing implies higher dissipation energy and dielectric losses. These results are consistent with the significant rise in dielectric constant and conductivity observed in the AC measurements (Fig 4(a & d)). The position of maxima occurs near ---- kHz indicating low relaxation time compared to that of ZSM-5.

7 Sensing mechanism

Schematic diagram, presenting gas sensing mechanism, is shown in Fig. 5. Initially, acetone molecules get adsorbed onto the surface of NaA zeolite due to its high surface area and porosity.

NaA Zeolite + CH_3 C=OCH_3 → NaA Zeolite·CH_3 C=OCH_3

This is followed by interaction of acetone with the exchangeable sodium cations (Na+) within the zeolite framework, leading to polarization and charge transfer processes.

Na^++ CH_3 C=OCH_3 → Na+···CH_3 C=OCH_3

The interaction might result in the formation of complexes between the acetone molecules and the

sodium cations, modifying the local electronic environment of the zeolite.

NaA Zeolite·CH_3 C=OCH_3 → (Na+···CH_3 C=OCH_3) ·Zeolite

Na_{12} Si_{12} Al_{12} O_{48} $27H_2$ O + CH_3 C=OCH_3 → (Na+···CH_3 C=OCH_3)·Na_{12} Si_{12} Al_{12} O_{48} ·$27H_2$ O

The described mechanism involves adsorption of acetone molecules and interaction with sodium cations within the NaA zeolite, resulting in the formation of complexes. These complexes alter the optical and dielectric properties, which can be measured and used to detect the presence of acetone in environment.

8 Conclusion

The study effectively demonstrates the potential of Nano NaA zeolite as a highly efficient material for acetone detection. Comprehensive characterization using XRD, FTIR, TG-DTA, SEM, EDAX, and AFM confirms the zeolite's crystalline structure, presence of typical functional groups, thermal stability, porous morphology of the zeolite. The fabricated NaA zeolite sensor exhibits outstanding performance with a rapid response time of 88 seconds and a recovery time of 75 seconds at an optimal operating temperature of 75 °C. Sensitivity test reveals excellent detection capabilities at a saturation concentration of 85 ppm, with consistent performance across multiple trials and long-term stability over 30 days.

Additionally, the study of optical and dielectric properties through UV-Vis spectroscopy and dielectric measurements indicates significant changes upon acetone exposure, highlighting the sensor's interaction with acetone molecules. These findings underscore the sensor's high sensitivity, durability, and potential for real-time acetone monitoring in various applications, including environmental and medical diagnostics. The research validates nano NaA zeolite as a promising candidate for developing robust, low-cost, and efficient acetone sensor contributing to enhanced environmental monitoring and improved public health safety.

References

1 Guidotti T L, *Environ Res*, 15 (1978) 443.
2 Patil M A, Ganbavle V V, Rajpure K Y, Deshmukh H P & Mujawar S H, *Mater Sci Energy Technol*, 3 (2020) 36.
3 Han S, Huang W, Shi W & Yu J, *Sens Actuators B: Chem*, 203 (2014) 9.
4 Yang Z, Han S, Liu Y, Zhuang X, Akinwande D & Yu J, *Org Electron*, 62 (2018) 114.
5 Dil E A, Ghaedi M, Asfaram A, Mehrabi F & Sadeghfar F, *J Indus Eng Chem*,74 (2019) 55.
6 Dil E A, Ghaedi M, Asfaram A, Mehrabi F, Bazrafshan A A & Tayebi L, *Ultrason Sonochem*, 58 (2019) 104702.
7 Mehrabi F & Dil E A, *Ultrason Sonochem*, 37 (2017) 37.
8 Kiani M, Bagheri S, Karachi N & Dil E A, *Desalinat Water Treat*, 152 (2019) 366.
9 Huang X, Meng F, Sun Y & Liu J, *Sens Mater*, 17 (2005) 29.
10 Chen Y, Qin H, Cao Y, Zhang H & Hu J, *Sensors*, 18 (2018) 3425.
11 Heilig A, Barsan N, Weimar U & Göpel W, *Sens Actuators B: Chem*, 58 (1999) 302.
12 Aigner R, Auerbach F, Huber P, Müller R & Scheller G, *Sens Actuators B: Chem*, 18 (1994) 143.
13 Zehiroglu1 C & Sarikaya S B O, *J Food Sci Technol*, 56 (2019) 4757.
14 Fang L, Norris C, Johnson K, Cui X, Sun J, Teng Y, Tian E, Xu W, Li Z, Mo J, Schauer J J, Black M, Bergin M, Zhang J & Zhang Y, *Build Environ*, 157 (2019) 309.
15 Bortnovsky O, Dědeček J, Tvarůžková Z, Sobalík Z & Šubrt J, *J Am Ceram Soc*, 91 (2008) 3052.
16 Sun Y, Wang J, Li X, Du H, Huang Q & Wang X, *Sensors*, 18 (2018) 390.
17 Huang H, Zhou J, Chen S, Zeng L & Huang Y, *Sens Actuators B: Chem*, 101 (2004) 316.
18 Varsani P, Afonja A, Williams D E, Parkin I P & Binions R, *Sens Actuators B: Chem*, 160 (2011) 475.
19 Vilaseca M, Coronas J, Cirera A, Cornet A, Morante J R & Santamaria J, *Sens Actuators B: Chem*, 124 (2007) 99.
20 Sazama P, Jirglová H & Dědeček J, *Mater Lett*, 62 (2008) 4239.
21 Lv R, Zhang Q, Wang W, Lin Y & Zhang S, *Sensors (Basel)*, 21 (2021) 4069.
22 Li G, Cheng Z, Xiang Q, Yan L, Wang X & Xu J, *Sens Actuators B: Chem*, 283 (2019) 590.
23 Chen Y, Qin H, Wang X, Li L & Hu J, *Sens Actuators B: Chem*, 235 (2016) 56.
24 Zhang D, Liu A, Chang H & Xi B, *RSC Adv*, 5 (2015) 3016.
25 Haick H, Broza Y Y, Mochalski P, Ruzsanyibc V & Anton A, *Chem Soc Rev*, 43 (2014) 1423.
26 Buszewski B, Ulanowska A, Ligor T, Denderz N & Amann A, *Biomed Chromatogr*, 23 (2009) 551.
27 Choi S J, Fuchs F, Demadrille R, Grévin B, Jang B H, Lee S J, Lee J H, Tuller H L & Kim I D, *ACS Appl Mater Interf*, 6 (2014) 9061.
28 Jang J S, Koo W T, Choi S J & Kim I D, *J Am Chem Soc*, 139 (2017) 11868.
29 Koo W T, Jang J S, Choi S J, Cho H J, Kim I D, *ACS Appl Mater Interf*, 9 (2017) 18069.
30 Xiao J, Diao K, Zheng Z & Cui X, *J Mater Sci Mater Electron*, 29 (2018).
31 Wakade M D, Naik K B, Kutte V D, Narwade V N, Lakhane M A, Bogle K A, Khairnar R S, Mahabole M P, *Mater Today Proc*, 92 (2023) 933.
32 Lakhane M, Khairnar R & Mahabole M, *Bull Mater Sci*, 39 (2016) 1483.
33 Kutte V, Naik K, Lakhane M, Wakade M, Waghmare P, Sabale P & Mahabole M, 92 (2023) 960.
34 Khairnar R S, Wakde M D, Mahabole M P, Krishna R& Titus E, *Int J Eng Innovat Technol (IJEIT)*, 3 (2014) 306.